High-Frequency EPR Study of a New Mononuclear Manganese(III) Complex: [(terpy)Mn(N_3)$_3$] (terpy = 2,2′:6′,2″-Terpyridine)

Julian Limburg,[†,1a] John S. Vrettos,[1a] Robert H. Crabtree,[1a] Gary W. Brudvig,[1a] Julio C. de Paula,[1b] Alia Hassan,[1c] Anne-Laure Barra,[1c] Carole Duboc-Toia,*[,1c] and Marie-Noëlle Collomb*[,1d]

Department of Chemistry, Yale University, P.O. Box 208107, New Haven, Connecticut 06520-8107, Department of Chemistry, Haverford College, 370 Lancaster Avenue, Haverford, Pennsylvania 19041, Grenoble High Magnetic Field Laboratory, CNRS-MPI, BP 166, 38042 Grenoble Cedex 9, France, and Laboratoire d'Electrochimie Organique et de Photochimie Rédox, CNRS UMR 5630, Université Joseph Fourier, BP 53, 38041 Grenoble Cedex 9, France

Received October 10, 2000

The isolation and structural characterization of [(terpy)$Mn^{III}(N_3)_3$], complex **1**, is reported (terpy = 2,2′:6′,2″-terpyridine). Complex **1**, a product of the reaction between the mixed-valence dimer [(terpy)$(H_2O)Mn^{III}(O)_2$-$Mn^{IV}(OH_2)$(terpy)]$(NO_3)_3$ and NaN_3, crystallizes in a triclinic system, space group $P\bar{1}$, a = 8.480(1) Å, b = 8.9007(2) Å, c = 12.109(2) Å, α = 93.79(1)°, β = 103.17(1)°, γ = 103.11(1)°, and Z = 2. Complex **1** exhibits a Jahn−Teller distortion of the octahedron characteristic of a six-coordinated high-spin Mn(III). A vibrational spectroscopic study was performed. The $\nu_{asym}(N_3)$ mode of complex **1** appears in the IR as a strong band at 2035 cm^{-1} with a less intense feature at 2072 cm^{-1}, and in the FT-Raman as a strong band at 2071 cm^{-1} with a weaker broad band at 2046 cm^{-1}. The electronic properties of complex **1** were investigated using a high-field and high-frequency EPR study (190−475 GHz). The different spin Hamiltonian parameters have been determined (D = −3.29 (±0.01) cm^{-1}, E = 0.48 (±0.01) cm^{-1}, E' = 0.53 (±0.01) cm^{-1}, g_x = 2.00 (±0.005), g_y = 1.98 (±0.005), g_z = 2.01 (±0.005)). These parameters are in agreement with the geometry of complex **1** observed in the crystal structure, a $D < 0$ related to the elongated distortion, and a value of E/D close to 0.2 as expected from the highly distorted octahedron. The two values of the E-parameter are explained by the presence of two slightly different structural forms of complex **1** in the crystal lattice. A second hypothesis was explored to explain the experimental data. The calculation for the simulation was done taking into account that the **g** and **D** tensors are not collinear due to the low symmetry of complex **1**. In that case, the spin Hamiltonian parameters found are D = −3.29 (±0.01) cm^{-1}, E = 0.51 (±0.01) cm^{-1}, g_x = 2.00 (±0.005), g_y = 1.98 (±0.005), and g_z = 2.01 (±0.005).

Introduction

Manganese superoxide dismutase (MnSOD), an enzyme present in different organisms, is located in the chloroplast and mitochondria of eukaryotes and in the cytoplasm of bacteria.[2] It is an antioxidant protein that catalyzes the dismutation of the superoxide radical with a mononuclear Mn(III) complex at the active site. This enzyme is inhibited by a variety of molecules, including oxidants[3] or small anions such as azide.[4] In all cases, the Mn(III) ion is thought to be the site of inhibition. Thus, a complete analysis of the electronic properties of the manganese ion is necessary in order to understand the role of the metal in those processes. Mn(III) is a high-spin d^4 ion resulting in a S = 2 spin ground state. The special feature of non-Kramers systems is that, in zero field, the spin ground state multiplet is split and large zero-field splittings (zfs) are expected for Mn(III) complexes as a result of the low symmetry due to Jahn−Teller distortions from an octahedral geometry. This results in the absence of any EPR signals at classical frequency (X-band) because no signal can be observed if the zfs is much larger than the microwave quantum used in the spectrometer. For this reason, Mn(III) is one of the least favorable metal ions for EPR study.

A recent study in parallel polarization EPR at X-band frequency, which allows observation of transitions between closely spaced $M_s = \pm 2$ energy levels, determined the different spin Hamiltonian parameters of the MnSOD of *Thermus thermophilus*. According to eq 1, the zfs parameters are represented by the last two terms, where D and E correspond to the axial and the rhombic parts of the interaction, respectively. It has been found that D = +2.10 cm^{-1} and E = 0.24 cm^{-1}.[4]

$$H = \beta \mathbf{B} \mathbf{g} \mathbf{S} + D[S_z^2 - (1/3)S(S+1) + (E/D)(S_x^2 - S_y^2)] \quad (1)$$

In this previous study,[4] the parallel polarization EPR technique was efficient because the D value of the Mn(III) ion is not very large. However, upon azide binding, no EPR signal

* To whom correspondence should be addressed: toia@labs.polycnrs-gre.fr, fax 33 4 76 85 56 10; and Marie-Noelle.Collomb@ujf-grenoble.fr, fax 33 4 76 51 42 67.

† Current address: Department of Chemistry, University of California−Berkeley, Berkeley, CA 94720.

(1) (a) Department of Chemistry, Yale University. (b) Department of Chemistry, Haverford College. (c) Grenoble High Magnetic Field Laboratory. (d) Laboratoire d'Electrochimie Organique et de Photochimie Rédox, Université Joseph Fourier.

(2) Fridovich, I. *Annu. Rev. Biochem.* **1995**, *64*, 97−112.

(3) MacMillan-Crow, L. A.; Crow, J. P.; Thompson, J. A. *Biochemistry* **1998**, *37*, 1613−1622.

(4) Campbell, K. A.; Yikilmaz, E.; Grant, C. V.; Gregor, W.; Miller, A.-F.; Britt, R. D. *J. Am. Chem. Soc.* **1999**, *121*, 4714−4715.

10.1021/ic001118j CCC: $20.00
Published on Web 03/02/2001

could be observed due to an increase of the *D* value. Also, a change of the sign is predicted on the basis of magnetic circular dichroism studies.[5] For the azide-bound system, high-field and high-frequency EPR (HF-EPR) seems to be required to obtain EPR spectra.

HF-EPR spectroscopy has been very successfully applied to the investigation of mononuclear metal ions with integer-spin states such as Fe(II),[6] Cr(II),[7] Mn(III),[8,9] and Ni(II);[10,11] of binuclear complexes with resulting integer-spin[12] or high-spin[13] ground states; and of high-spin polynuclear transition metal ion clusters also named nanomagnets.[14,15]

We describe here the isolation, structural characterization, and electronic properties, determined by a multifrequency EPR study, of a new mononuclear Mn(III) complex containing three azide ligands as a model of the MnSOD azide-binding active site. A vibrational spectroscopic study is also reported which characterizes the Mn−N vibrations in this complex. This complex was chosen to illustrate the efficiency of the HF-EPR technique for the study of such mononuclear Mn(III) systems even if the symmetry is very low due to strong distortions of the octahedron.

Experimental Section

All chemicals were purchased from Aldrich and used without further purification. [(terpy)(H_2O)Mn^{III}(O)$_2$$Mn^{IV}$($H_2O$)(terpy)]($NO_3$)$_3$ (terpy = 2,2′:6′,2″-terpyridine) was synthesized as described in the literature.[16,17] $KHSO_5$ was standardized by iodometric titration.

Synthesis of [(terpy)Mn^{III}(N_3)$_3$] (Complex 1). To a stirred solution of $Mn(OAc)_2$·$4H_2O$ (55 mg, 0.214 mmol) and 2,2′:6′,2″-terpyridine (50 mg, 0.214 mmol) in 0.1 M OAc/HOAc buffer (5 mL, pH = 4.5) was added potassium peroxomonosulfate (56 mg, 0.160 mmol in 2 mL buffer), to give a green solution of [(terpy)(H_2O)Mn(O)$_2$Mn(OH_2)-(terpy)]$^{3+}$. On addition of 1 mL of a saturated NaN_3 solution and cooling in an ice bath, a dark brown precipitate of complex **1** was formed, which then was filtered, washed with water and dried in vacuo. **CAUTION: both N_3^- and its complexes are potentially explosive. Although we have encountered no such problems with complex 1, it should still be handled with care. Further, N_3^- releases explosive HN_3 on contact with acid solution**. The complex was recrystallized from acetonitrile to give black needle crystals, yield = 53 mg (60%). Elemental anal. Calcd for complex **1** ($C_{15}H_{11}N_{11}Mn$): C, 43.48; H, 2.66; N, 40.58. Found: C, 42.90; H, 2.70; N, 39.77. IR (KBr): 3440 (s, br), 2072 (s), 2035 (vs), 1595 (m), 1575 (m), 1451 (m), 1358 (m), 1299 (m), 773 (s), 646 (w), 628 (w). FT-Raman (N_3 modes) (KBr): 2069 (s), 1302 (m), 1294 (m), 357 (s, b), 345 (sh).

Physical Measurements. UV/vis spectra were recorded on an HP 8453 diode-array UV−visible spectrophotometer. FT-IR spectra were taken on a Midac Corporation M series spectrophotometer. FT-Raman spectra were recorded on a Nicolet 950 spectrophotometer with excitation at 1064 nm from a Nd:YVO_4 laser, and incident power of 100 mW. Spectral deconvolutions were performed using Origin (v. 6.0, Microcal Software Inc.) and Microsoft Excel (v. 8.0, Microsoft Inc.). High-frequency and high-field EPR spectra were recorded on a laboratory-made spectrometer[18,19] using powder samples pressed in pellets to avoid preferential orientation of the crystallites in the strong magnetic field. Gunn diodes operating at 95 and 115 GHz and equipped with a second-, third-, fourth-, and fifth-harmonic generator have been used as radiation source. Two types of magnets were also used to produce the magnetic field, a superconducting magnet (0−12 T) and a resistive magnet (0−23 T).

Crystal Structure Determination of Complex 1. A crystal of complex **1** of dimensions 0.05 × 0.19 × 0.24 mm was selected from the bulk recrystallization from acetonitrile. Diffraction data were collected on an Enraf-Nonius CAD-4 diffractometer with graphite-monochromated Mo Kα radiation, and the crystallographic data are summarized in Table 1. The structure was solved by standard Patterson methods, using the SHELXS computer program.[20] The non-hydrogen atoms were refined anisotropically, and hydrogen atoms were located in the difference map and refined isotropically. All calculations were performed using the TEXSAN crystallographic software package of Molecular Structure Corporation.[21] The full details of the X-ray structure determination can be found in the Supporting Information.

Table 1. Summary of Crystallographic Data and Parameters for [(terpy)Mn^{III}(N_3)$_3$], Complex **1**

chemical formula	$C_{15}H_{11}N_{12}Mn$
fw	414.27
cryst syst	triclinic
space group (No.)	$P\bar{1}$ (2)
a (Å)	8.480(1)
b (Å)	8.907(2)
c (Å)	12.109(2)
α (deg)	93.79(1)
β (deg)	103.17(1)
γ (deg)	103.11(1)
V (Å^3)	860.7
T (°C)	−90.0
λ (Å)	0.71069
δ_{calc} (g cm^{-3})	1.598
Z	2
F(000)	420.00
abs coeff, cm^{-1}	7.65
no. of reflns collcd/unique	3713/3486
no. of observations ($I > 3\sigma(I)$)	2694
no. of refined params	297
largest peak/hole, e Å^{-1}	0.50/−0.76
R^a	0.037
R_w^b	0.047

^{a} $R = \sum||F_o| - |F_c||/\sum|F_o|$. ^{b} $R_w = [(\sum w(|F_o| - |F_c|)^2/\sum wF_o^2)]^{1/2}$.

Results and Discussion

Synthesis and Crystal Structure of Complex 1. Complex **1** was obtained by the reaction between [(terpy)(H_2O)Mn^{III}(O)$_2$-Mn^{IV}(H_2O)(terpy)](NO_3)$_3$ (terpy = 2,2′:6′,2″-terpyridine)[16,17] and NaN_3 causing the binuclear species to dissociate into

(5) Whittaker, J. W.; Whittaker, M. M. *J. Am. Chem. Soc.* **1991**, *113*, 5528−5540.
(6) Knapp, M. J.; Krzystek, J.; Brunel, L.-C.; Hendrickson, D. N. *Inorg. Chem.* **2000**, *39*, 281−288.
(7) Telser, J.; Pardi, L. A.; Krzystek, J.; Brunel, L.-C. *Inorg. Chem.* **1998**, *37*, 5769−5775.
(8) Barra, A.-L.; Gatteschi, D.; Sessoli, R.; Abbati, G. L.; Cornia, A.; Fabretti, A. C.; Uytterhoeven, M. G. *Angew. Chem., Int. Ed. Engl.* **1997**, *36*, 2329−2331.
(9) Krzystek, J.; Telser, J.; Pardi, L. A.; Goldberg, D. P.; Hoffman, B. M.; Brunel, L.-C. *Inorg. Chem.* **1999**, *38*, 6121−6129.
(10) Van Dam, P. J.; Klaasen A. A. K.; Reijerse, E. J.; Hagen, W. R. *J. Magn. Reson.* **1998**, *130*, 140−144.
(11) Pardi, L. A.; Hassan, A. K.; Hulsbergen, F. B.; Reedijk, J.; Spek, A. L.; Brunel, L.-C. *Inorg. Chem.* **2000**, *39*, 159−164.
(12) Duboc-Toia, C.; Hummel, H.; Bill, E.; Barra, A.-L.; Chouteau, G.; Wieghardt, K. *Angew. Chem., Int. Ed.* **2000**, *39*, 2888−2890.
(13) Knapp. M. J.; Krzystek, J.; Brunel, L.-C.; Hendrickson, D. N. *Inorg. Chem.* **1999**, *38*, 3321−3328.
(14) Barra, A.-L.; Brunel, L.-C.; Gatteschi, D.; Pardi, L. A.; Sessoli, R. *Acc. Chem. Res.* **1998**, *31*, 460−466.
(15) Barra, A.-L.; Caneschi, A.; Cornia, A.; Fabrizi de Biani, F.; Gatteschi, D.; Sangregorio, C.; Sessoli, R.; Sorace, L. *J. Am. Chem. Soc.* **1999**, *121*, 5302−5310.
(16) Collomb, M.-N., Deronzier, A.; Richardot, A.; Pecaut, J. *New J. Chem.* **1999**, *23*, 351−353.
(17) Limburg, J.; Vrettos, J. S.; Liable-Sands, L. M.; Rheingold, A. L.; Crabtree, R. H.; Brudvig, G. W. *Science* **1999**, *283*, 1524−1527.
(18) Barra, A.-L.; Brunel, L.-C.; Robert, J. B. *Chem. Phys. Lett.* **1990**, *165*, 107−115.
(19) Muller, F.; Hopkins, M. A.; Coron, N.; Grynderg, M.; Brunel, L.-C.; Martinez, G. *Rev. Sci. Instrum.* **1989**, *60*, 3681−3684.
(20) Sheldrick, G. M. In *Crystallographic Computing 3*; Sheldrick, G. M., Krüger, C., Goddard, R., Eds.; Oxford University Press, 1985; pp 175−189.
(21) *TEXSAN*, Single Crystal Structure Analysis Software, version 5.0; Molecular Structure Corporation: The Woodlands, TX, 1989.

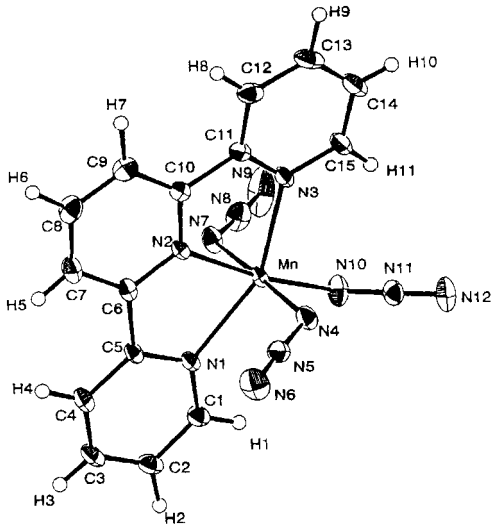

Figure 1. ORTEP diagram of [(terpy)$Mn^{III}(N_3)_3$], complex **1**.

mononuclear complexes. This reaction demonstrates the lability of the di-μ-oxo core in the binuclear Mn(III) Mn(IV) complex even though the distance between the two metallic ions is short (Mn···Mn = 2.7 Å). This lability was already observed in the case of the binuclear μ-oxo-di-μ-acetato Mn(III) complex.[22]

Complex **1** is soluble in acetonitrile, from which X-ray quality crystals can be obtained. Figure 1 shows the structure of this new mononuclear Mn(III) complex: [(terpy)$Mn^{III}(N_3)_3$]. The Mn(III) ion exhibits a highly distorted octahedral coordination sphere, with three nitrogen atoms of azido groups (Mn−N4, Mn−N7, Mn−N10: 1.965(2), 1.987(2), 1.959(3) Å) and one nitrogen atom of the terpy ligand (Mn−N2: 2.109(3) Å) defining the equatorial plane. The presence in the equatorial plane of one nitrogen atom from the terpy ligand causes a distortion of the octahedron because the Mn−terpy bond is longer than the Mn−azide bonds. The axial positions are occupied by the two other nitrogen atoms of terpy which display a tetragonal elongation as a result of the Jahn−Teller distortion expected for a high-spin Mn(III) complex (d^4) (Mn−N1, Mn−N3: 2.234(2), 2.258(2) Å). A similar tetragonal elongation is also observed in [(tacn)$Mn^{III}(N_3)_3$] (tacn = 1,4,7-triazacyclononane), where the distortion is along an $N_{azide}-Mn-N_{tacn}$ axis.[22]

The three $Mn-N_{azide}$ distances in complex **1** are approximately the same (av Mn···N_{azide} 1.970 Å), and are similar to the two equatorial $Mn-N_{azide}$ in [(tacn)$Mn^{III}(N_3)_3$] (av Mn··· N_{azide} 1.931 Å). For this latter complex, the Jahn−Teller elongated $Mn-N_{azide}$ axial distance is longer (2.170 Å).

Vibrational Spectroscopy. The vibrational spectra of Mn azide complexes have been studied with the spectra assigned directly by ^{15}N-labeling,[23] and also by comparison with other metal azide complexes.[24] The $\nu_{asym}(N_3)$ mode of complex **1** is easily observed and assigned, appearing in the IR as a strong band at 2035 cm^{-1} with a less intense feature at 2072 cm^{-1}, and in the FT-Raman as a strong band at 2071 cm^{-1} with a weaker broad band at 2046 cm^{-1}. The frequencies of the $\nu_{asym}(N_3)$ mode in complex **1** are similar to those observed for [(Me_3-tacn)$Mn^{V}(N)(N_3)_2$] (Me_3-tacn = 1,4,7-trimethyl-1,4,7-triazacyclononane) (2063 and 2032 cm^{-1}),[25] [(bpy)$Mn^{IV}(N_3)_4$] (2055 and 2038 cm^{-1}),[23] *trans*-[(cyclam)$Mn^{III}(N_3)_2$](ClO_4) (cyclam = 1,4,8,11-tetraazacyclotetradecane) (2069 and 2046 cm^{-1}),[25] and [(Me_3-tacn)$Mn^{III}(N_3)_3$] (2067 and 2027 cm^{-1}).[25] It was shown by comparison of the crystal structures and IR spectra of a series of Cu, Zn, and Cd azide complexes that the splitting of the intra-azide bands is a result of asymmetry, requiring there to be at least two distinct azides.[26] This reasoning was also used to explain the splitting of the $\nu(N_3)$ bands in the resonance Raman spectrum of [(bpy)$Mn^{IV}(N_3)_4$].[23] Inspection of the crystal structure of complex **1** (Table 2) reveals such asymmetry among the azide ligands, with one ligand having shorter N−N bond lengths than the other two. It should be noted that *trans*-[(cyclam)$Mn^{III}(N_3)_2$](ClO_4)[25] is an apparent exception to this rule as the azide ligands are crystallographically identical. [(Me_3-tacn)$Mn^{III}(N_3)_3$] and [(Me_3-tacn)$Mn^{V}(N)(N_3)_2$] have not been crystallographically characterized.[25]

Table 2. Selected Bond Angles (deg) and Distances (Å) for [(terpy)$Mn^{III}(N_3)_3$], Complex **1**

Mn−N(1)	2.234(2)	N(4)−N(5)	1.206(3)
Mn−N(2)	2.109(2)	N(7)−N(8)	1.182(3)
Mn−N(3)	2.258(2)	N(10)−N(11)	1.204(3)
Mn−N(4)	1.965(2)	N(5)−N(6)	1.146(4)
Mn−N(7)	1.987(2)	N(8)−N(9)	1.141(4)
Mn−N(10)	1.959(3)	N(11)−N(12)	1.147(3)
N(1)−Mn−N(2)	74.37(8)	Mn−N(7)−N(8)	123.6(2)
N(1)−Mn−N(3)	148.30(9)	N(7)−N(8)−N(9)	176.5(4)
N(1)−Mn−N(4)	90.40(9)	Mn−N(10)−N(11)	120.9(2)
N(1)−Mn−N(7)	87.37(9)	N(10)−N(11)−N(12)	177.3(3)
N(1)−Mn−N(10)	112.5(1)	N(4)−N(5)−N(6)	177.0(3)
N(2)−Mn−N(3)	73.93(8)	N(2)−Mn−N(4)	92.27(9)
N(2)−Mn−N(7)	88.37(9)	N(2)−Mn−N(10)	172.8(1)

In addition to the anti-symmetric stretch, manganese terminal azide complexes are expected to display $\nu_{sym}(N_3)$ modes in their IR[24,25] and Raman[23] spectra at ∼1300−1350 cm^{-1}, a deformation mode, $\delta(N_3)$, in the IR at ∼620 cm^{-1}, and a $\nu(MnN_3)$ mode in the Raman at ∼350 cm^{-1}. These may also be split due to the asymmetry of the azide ligands.[23] The $\nu_{sym}(N_3)$ mode appears at 1358 and 1299 cm^{-1} in the IR; this mode is seen as a strong band at 1333 cm^{-1} and a weaker, broader band at 1346 cm^{-1} in the Raman. The deformation mode is seen in the IR at 646 and 628 cm^{-1}. The lowest frequency mode, the $\nu(MnN_3)$ stretch, depends on the oxidation state of the metal.[23] This mode is observed in the FT-Raman as a strong band at 349 cm^{-1} with shoulders at 343 and 355 cm^{-1}. Again, the splitting arises from differences in the Mn−N bond lengths.

High-Frequency EPR Spectroscopy. Complex **1** is EPR "silent" at low frequency (X-band) as expected for a Mn(III) mononuclear complex. The HF-EPR experiments were performed on polycrystalline powder samples of complex **1** over a temperature range of 5 to 15 K. The system presents a very large zfs. Therefore, it is necessary to perform a multifrequency EPR study (190−475 GHz) as shown in Figures 2 and 3, where all the spectra were recorded at 5 K. A signal is observed at $g = 2$ which is attributed to an impurity (Figure 2D at ∼8.0 T and Figure 3A at ∼10.2 T).

Complex **1** is rhombic, as revealed by the presence of three types of transitions that are associated with the *x*, *y*, and *z* axes. The two transitions at 13.3 and 17.9 T in Figure 3A, which are at higher fields than $g = 2$ (∼10.2 T) in the 285 GHz spectrum, are identified as transitions along the *y*- and *x*-axis, respectively.

(22) Wieghardt, K.; Bossek, U.; Nuber, B.; Weiss, J. *Inorg. Chim. Acta* **1987**, *126*, 39−43.
(23) (a) Dave, B.G; Czernuszewicz, R. S. *J. Coord. Chem.* **1994**, *33*, 257−269. (b) Czernuszewicz, R. S.; Wagner, W.-D.; Ray, G. B.; Nakamoto, K. *J. Mol. Struct.* **1991**, *242*, 99.
(24) Cortés, R.; Pizarro, J. L.; Lezama, L.; Arriortua, M. I.; Rojo, T. *Inorg. Chem.* **1994**, *33*, 2697−2700.
(25) Meyer, K.; Bendix, J.; Metzler-Nolte, N.; Weyhermüller, T.; Wieghardt, K. *J. Am. Chem. Soc.* **1998**, *120*, 7260−7270.
(26) Agreel, I. *Acta Chem. Scand.* **1971**, *25*, 2965.

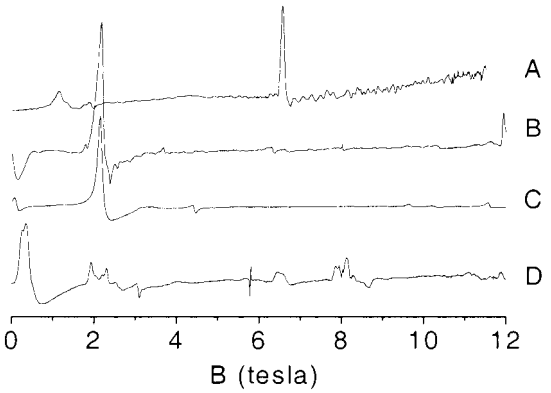

Figure 2. Experimental (A, B, and D) and simulated (C) powder HF-EPR spectra of polycrystalline complex **1** measured at 475 GHz (A), 345 GHz (B and C), and 230 GHz (D). The spectra were recorded at 5 K on a superconducting magnet. The parameters used for the simulation are $D = -3.29$ cm^{-1}, $E = 0.48$ cm^{-1}, $g_x = 2.00$, $g_y = 1.98$, $g_z = 2.01$.

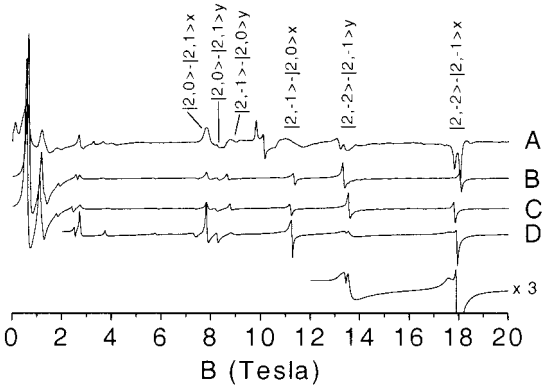

Figure 3. Experimental (A) and simulated (B, C, and D) powder HF-EPR spectra of polycrystalline complex **1** measured at 285 GHz. The spectra were recorded at 5 K on a resistive magnet. The parameters used for the simulation are (B) $D = -3.29$ cm^{-1}, $E' = 0.53$ cm^{-1}, $g_x = 2.00$, $g_y = 1.98$, $g_z = 2.01$; (C) $D = -3.29$ cm^{-1}, $E = 0.48$ cm^{-1}, $g_x = 2.00$, $g_y = 1.98$, $g_z = 2.01$; (D) $D = -3.29$ cm^{-1}, $E = 0.51$ cm^{-1}, $\theta = 12°$, $g_x = 2.00$, $g_y = 1.98$, $g_z = 2.01$. The allowed transitions of the quintuplet are labeled on the experimental spectrum A.

These two features each present an unusual doublet shape that we will discuss later (17.14 and 18.05 T at 285 GHz for the *x*-component). The transition observed at low field (2.15 T at 345 GHz and 6.5 T at 475 GHz) corresponds to a transition along the *z*-axis (Figure 2).

The "allowed" character of the three previous transitions was confirmed by following the effect of the frequency on their field position (Figure 4). The experimental data could be fitted linearly in each case with *g*-values close to $g = 2$ and are in good agreement with a Mn(III) ion for which all the different components of the **g**-tensor are expected to be close to $g = 2$. They can be completely assigned from the temperature dependence of their relative intensities. The intensity of these three transitions decreases with increasing temperature. Because at low temperature only the $|S, M_s\rangle = |2, -2\rangle$ level is significantly populated, low-temperature spectra correspond mainly to the $|2, -2\rangle \rightarrow |2, -1\rangle$ transitions. Other allowed transitions of the quintuplet along the *x* and *y* axes are observed in the spectra recorded at 5 K. Their intensity increases at higher temperature (10 K). These features correspond to $|2, -1\rangle \rightarrow |2, 0\rangle$ and $|2, 0\rangle \rightarrow |2, 1\rangle$ transitions for the corresponding principal axes. They are less affected by the doublet shape observed for the $|2, -2\rangle \rightarrow |2, -1\rangle$ transitions. Nevertheless, the $|2, -1\rangle \rightarrow |2, 0\rangle$ transition along *x* is broadened. As shown in Figure 3A, at 285 GHz, the $|2, -1\rangle \rightarrow |2, 0\rangle$ transitions along *x* and *y* are observed respectively at 11.2 and 8.8 T, and the $|2, 0\rangle \rightarrow |2, 1\rangle$ transitions at 7.8 and 8.2 T. This assignment will be confirmed later (Figure 5).

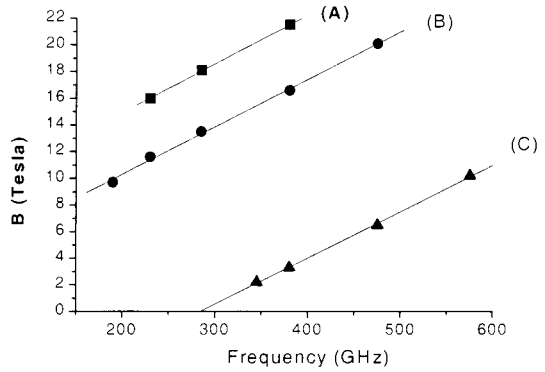

Figure 4. Resonant field versus frequency diagram for the $|2, -2\rangle \rightarrow |2, -1\rangle$ transitions along the *x*- (A), *y*- (B), and *z*- (C) axes.

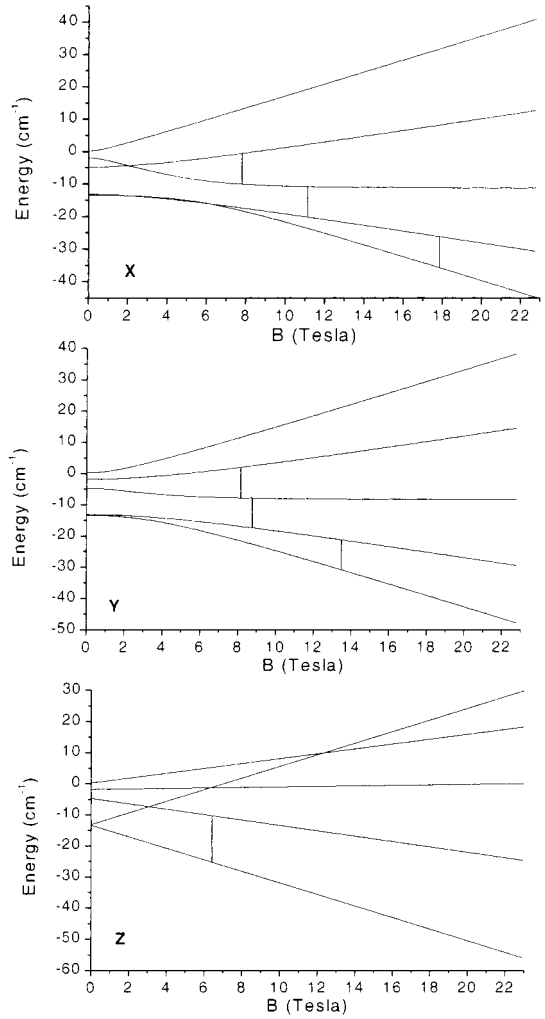

Figure 5. Plots of energy vs field for the five energy levels arising from an $S = 2$ spin state using the following parameters: $D = -3.29$ cm^{-1}, $E = 0.50$ cm^{-1}, $g_{iso} = 2.00$. The field is parallel to the molecular axis that is indicated in each frame. The observed resonances at 285 GHz are indicated by vertical bars along the *x*- and *y*-axes and at 475 GHz along the *z*-axis.

An important feature of low-temperature HF-EPR spectra is that they directly provide the sign of the zfs parameter *D*. Under these conditions, only the lowest M_s levels are populated. If

$D < 0$, the transitions along the *z*-axis are observed to the low-field side of $g = 2$, while the reverse is true for $D > 0$. Here, the presence of a feature associated with the *z*-component of the quintuplet at low field shows unambiguously that the sign of *D* is negative. That is in agreement with the presence of an elongated octahedron. It was shown that the sign of *D* in the case of a Mn(III) system is directly correlated with the nature of the Jahn−Teller distortion.[27]

The observation of the $|2, -2\rangle \rightarrow |2, -1\rangle$ transition along the *z*-axis allowed us to make a first evaluation of the value of *D*. In fact, the energy difference between this transition and the $g = 2$ resonance corresponds to $3|D|/g_z\beta$. This yields a field difference of 10.2 T, corresponding to a value of $|D|$ of about 3.2 cm^{-1} (Figure 3).

Other transitions could be observed in the different spectra. All these features are associated with "forbidden" transitions. Therefore, it is difficult to make a qualitative assignment. The presence of such transitions is characteristic of systems with large zfs. In this case, the mixing of the different energy levels allows these "forbidden" transitions to be observed at certain frequencies. As expected, they are present in the low-field part of the spectra where the strong-field limit is not met ($D \ll g\beta B$). The "forbidden" transitions are easily distinguished by following their field position as a function of the frequency. First, the experimental data could be fitted linearly with *g*-values much larger than 2. Second, they are present only in a certain frequency range. Third, their intensity decreases with increasing EPR frequency. For instance, one signal is observed at 3.2, 5.5, and 6.4 T at 115, 190, and 230 GHz, respectively, corresponding to a *g*-value of 3.4; this resonance disappears above 230 GHz. At 285 and 230 GHz, all the low-field features (<4 T) correspond to "forbidden" transitions. Above 345 GHz, there are only some small intensity features from "forbidden" transitions (0.2 T at 345 GHz and 0.7 T at 475 GHz) (Figure 2).

The HF-EPR spectra of complex **1** were simulated by using a full-matrix diagonalization procedure of the Hamiltonian (eq 1) for the $S = 2$ spin ground state. The best-simulated spectra are shown in Figures 2 and 3 at 345 and 285 GHz, respectively. The spin Hamiltonian parameters used for these simulations are $D = -3.29$ (±0.01) cm^{-1}, $E = 0.48$ (±0.01) cm^{-1}, $E' = 0.53$ (±0.01) cm^{-1}, $g_x = 2.00$ (±0.005), $g_y = 1.98$ (±0.005), $g_z = 2.01$ (±0.005). The calculated transitions are very sensitive to the zfs parameters both in value and in sign. The value and sign of the *D* parameter are close to the preliminary value calculated above (3.2 cm^{-1}). The two *E* values (*E* and *E'*) correspond to the values for each of the two species that contribute to the doublet shape of the *x*- and *y*-components of the quintuplet. It is possible to simulate this doublet shape by using only two discrete values of *E* because these transitions are the only ones really sensitive to this parameter *E*. It is clear that the difference between *E* and *E'* is very small, but it cannot be considered as an *E* strain because in this case only a broadening of the signal would be expected. The intensity, the position, and the shape of the principal features ("allowed" transitions) are in good agreement with the experimental data.

The system is rhombic with an *E*/*D* value of 0.15, as expected from the geometry around the metal ion in complex **1**. The angle between N1MnN3 of 148.30(9)° is displaced by about 30° from that expected for a purely axial system. Moreover, the asymmetry of the system is increased because of the difference in the lengths of the Mn−N bonds in the equatorial plane of the octahedron (see Table 2).

(27) Gerritsen, H. J.; Sabisky, E. S. *Phys. Rev.* **1963**, *132*, 1507−1512.

The Zeeman energy splittings of a $S = 2$ system along the three molecular axes were calculated and plotted in Figure 5 using the following parameters: $D = -3.29$ cm^{-1}, $E = 0.50$ cm^{-1}, $g_{iso} = 2.00$. In this figure, the Zeeman splitting when the field is parallel with each of the molecular axes, *X*, *Y*, and *Z*, is plotted in a separate frame. As expected with the high *E*/*D* value, the three splittings of the M_s levels are very different along each axis. At low field, except along the *z*-axis, the relation between the energy of the M_s levels and the field is not linear. This induces level mixing which is the reason of the presence of "forbidden" transitions. In the high-field limit, the linear relation is again observed along the three principal axes.

A surprising observation for the different spectra is the doublet shape of the *x*- and *y*-components of the quintuplet. One possible explanation is that there are two slightly different structural forms of complex **1** in the crystal lattice. For the $P\bar{1}$ space group used to solve the crystal structure, two complexes in the crystal lattice are required by symmetry to be identical. To test whether these two complexes could be slightly different, the X-ray structure was also solved in the *P*1 space group, allowing an independent comparison of the two molecules of complex **1** present per unit cell. The small differences found in the metal−ligand bonds appear to be within the uncertainty of the structure. Therefore, it is difficult to attribute this doublet shape to a variable Jahn−Teller effect. Nevertheless, the structure was solved at room temperature and the HF-EPR measurements were recorded between 5 and 15 K, so we cannot completely eliminate the hypothesis that two structural forms of complex **1** are present in the lattice.

The second hypothesis comes from the low symmetry of complex **1**. We thus consider that the tensors **D** and **g** are not collinear. For the sake of simplicity, we conserve the hypothesis that the tensors remain collinear along *z* because the doublet shape of the signal only appears for the transitions along the *x* and *y* axes. We repeated the calculation with an additional parameter θ, where θ is the angle between the **D** and **g** tensors along *x* and *y*. The simulated spectrum, shown in Figure 3D, is obtained using the following parameters: $D = -3.29$ (±0.01) cm^{-1}, $E = 0.51$ (±0.01) cm^{-1}, $\theta = 12$ (±1)°, $g_x = 2.00$ (±0.005), $g_y = 1.98$ (±0.005), $g_z = 2.01$ (±0.005). The only parameters that are modified, compared to the previous calculations, are *E* and θ. The only transitions sensitive to this calculation are the *x* and *y* transitions of the quintuplet. This was confirmed with simulations done at other frequencies (data not shown). The $|2, -2\rangle \rightarrow |2, -1\rangle$ transitions are split into two components as in the experimental spectra. The intensity of the doublet shape is not completely reproduced in the simulation for the *x*-component but is in very good agreement for the *y*-component. The signals are sharper in this simulation than in Figure 3B and Figure 3C and allow the observation of the splitting of the transitions along the *x*-axis. Moreover, the relative intensity and the shape of the $|2, 0\rangle \rightarrow |2, 1\rangle$ transitions are better simulated. The simulated spectrum obtained with this new calculation provides convincing evidence in support of the hypothesis that the doublet character of the transitions along the *x*- and *y*-axes is due to noncollinearity of the **D** and **g** tensors. Nevertheless, a HF-EPR study on a single crystal is necessary to corroborate it and such measurements are planned for the near future when the size of the crystals will be acceptable for such study.

Conclusion

The lability of the di-μ-oxo Mn(III) Mn(IV) core was demonstrated by the reaction of $[(terpy)(H_2O)Mn^{III}(O)_2Mn^{IV}$-

(H_2O)(terpy)](NO_3)$_3$ with azide, yielding a new mononuclear Mn(III) complex containing azide ligands: [(terpy)Mn^{III}(N_3)$_3$]. IR and FT-Raman studies show that vibrational spectroscopy could be a useful probe for azide binding to Mn(III). It was also interesting to study the electronic properties of this complex considering its lack of symmetry. It is the first Mn(III) complex with such high rhombicity ($E/D = 0.15$) to be studied by HF-EPR spectroscopy. Most other Mn(III) complexes that have been studied by this technique are axial or nearly axial, although a six-coordinate Mn(III) complex, [Mn(dbm)$_3$] (Hdbm = 1,3-diphenyl-1,3-propanedione), was determined to have a moderate rhombicity ($E/D = 0.06$).[8] This work illustrates that, even in an unfavorable high-rhombicity case, a complete analysis could be performed. This demonstrates the importance of HF-EPR in studying the electronic properties of such systems. For metalloenzymes, such information is essential because the electronic structure of the metal ion can be directly correlated with the reactivity. In the case of MnSOD, the ability of the active site to bind small molecules and its redox chemistry are directly related to the electronic properties of the metal ion. Furthermore, the accurate determination of the different spin Hamiltonian parameters required in order to observe small differences between different forms of the enzyme is not possible due to the lack of effective methods. In this context, HF-EPR spectroscopy seems to be the appropriate technique, and experiments on biological samples are in progress.

Acknowledgment. This work was partially funded by the National Institutes of Health (Grant GM32715). M.-N.C. would like to thank NATO and the Centre National de la Recherche Scientifique for financial support. The authors thank Susan de Gala for solving the crystal structure of complex **1**.

Supporting Information Available: Crystallographic details for complex **1**. X-ray crystallographic files in CIF format for complex **1**. This material is available free of charge via the Internet at http://pubs.acs.org.

IC001118J